D/4

# A MULTIFREQUENCY EVALUATION OF ACTIVE AND PASSIVE MICROWAVE SENSORS FOR OIL SPILL DETECTION AND ASSESSMENT

Richard G. Fenner
National Aeronautics and Space Administration
Lyndon B. Johnson Space Center
Houston, Texas

Stephen C. Reid and Charles H. Solie
Lockheed Engineering and Management Services Company, Inc.
Houston, Texas

## ABSTRACT

During 1979, two major accidental oil spills occurred in the Gulf of Mexico. On June 3, 1979, the PEMEX well, Ixtoc I, suffered a blow-out and was not capped until the spring of 1980. On November 1, 1979, the freighter Mimosa collided with the tanker Burma-Agate at the entrance to the Port of Galveston. Five to six of the Burma-Agate's tanks were ruptured. Fire resulting from the collision prevented them from being sealed, and several thousand barrels of crude oil were subsequently spilled into the Gulf. These spills presented a major ecological threat to the Texas Gulf Coast, but offered a unique opportunity to evaluate multiple-frequency microwave sensor data for oil-spill detection and assessment.

During the summer of 1979, the NASA/Lyndon B. Johnson Space Center was evaluating an X-band synthetic aperture radar (X-SAR) system on a NASA WB-57 high-altitude aircraft. Imagery of the Ixtoc I spill was obtained on June 3, 1979, in a flight over the Gulf of Mexico, east of Harlingen, Texas. In November, the NASA Earth Survey #2 C-130 aircraft was being made ready for a data-gathering mission. As part of the premission sensor evaluation, several runs were made over the Burma-Agate spill gathering active/passive microwave and multispectral scanner data. In January 1980, an additional C-130 aircraft active/passive microwave data flight was made over the Ixtoc I well oil spill. Supportive photographic data was taken on these C-130 flights.

This paper will present an evaluation of the data gathered on these flights with respect to how active and passive microwave sensors can best be used in oil-spill detection and assessment. Radar backscatter curves taken over oil spills will be presented and their effect on synthetic aperture radar (SAR) imagery will be discussed. Plots of microwave radiometric brightness variations over oil spills will be presented and discussed. Recommendations as to how to select the best combination of frequency, viewing angle, and sensor type for evaluation of various aspects of oil spills will also be discussed.

## INTRODUCTION

Numerous studies[1-13] have been conducted which have firmly established the ability of remote sensors to define the presence of oil slicks, their aerial coverage, temporal development and spectral reflectance and emission characteristics.

The effect of oil spilled on the surface of the sea is to dampen the very short capillary waves that dominate microwave radar backscatter. Consequently, the use of radar for observing oil spills has been the subject of considerable experimental effort over the last several years. The oil-spill observation is ordinarily done with an aircraft-mounted imaging radar capable of displaying signals from the sea-surface wave patterns. A dark area on the image indicates the absence of capillary waves, and consequently, the presence of oil spills.

Since radar intrinsically possesses the all-weather, day/night capability and the large swath widths required for timely continuous monitoring of oil contamination of the ocean surface, an orbital radar system is a likely candidate for worldwide monitoring of oil spills.

Unfortunately, quantitative research into the amount of radar backscatter suppression due to the phenomenon has been too little to adequately predict performance of operational radar oil-spill monitoring systems.

Early studies[14] conducted by the Naval Research Laboratory concluded that viewing angles greater than 45 degrees off nadir should be used to avoid specular returns and provide maximum swath widths for aircraft-mounted imaging radars.

Contrasted to the aircraft situation where incidence angle ranges of 45 degrees or greater are usually required to obtain reasonable swaths, a spacecraft incidence angle range of only a few degrees (Seasat case of five degrees at a 22-degree incidence angle) provides swaths of 100km or greater. This combined with allowable viewing angles and the ambiguity constraints of a spacecraft synthetic aperture radar (SAR) results in a need to well define the angular response of oilspill backscatter for various wavelengths to establish the system parameters for an orbital oilspill detection SAR.

K. Krishen[15] presented the analysis of 13.3 GHz scatterometer data gathered over a crude-oil spill off the Mississippi River Delta in the Gulf of Mexico. Krishen's results for a moderate sea state (wind speed of 18 knots) demonstrated that scatterometer systems can be used to detect oil spills at incidence angles less than 45 degrees off nadir and that the oil's smoothing of the sea results in a predictable decrease in the radar scattering coefficient.

This paper will present the results of analysis of the data taken on the previously mentioned aircraft flights. In analyzing the data, emphasis was placed on determining the optimum frequency and sensor for a spaceborne platform.

Before describing the results of this experiment, a brief review of the instrumentation and processing will be given to assist in the interpretation of the data presented in later sections of this paper.

## INSTRUMENTATION

The NASA/JSC WB-57 and C-130 aircraft are operated as part of the Airborne Instrumentation Research Program (AIRP). They are used to gather

remote sensing data for Earth Resources Applications investigations. In addition to active microwave sensors, both aircraft carry Zeiss color and color-infrared photographic equipment and multispectral scanners. The C-130 aircraft is instrumented with passive microwave radiometer systems and four active microwave sensors called scatterometers. These systems are continuous wave radars that illuminate the surface in a fan beam from nadir to 50 degrees aft of nadir along the flight path of the aircraft. The operating wavelengths are 75cm (400 MHz), 18.5cm (1.6 GHz), 6.3cm (4.75 GHz) and 2.3cm (13.3 GHz). The spatial resolutions are approximately 75mm x 180m, 40m x 120m, 40m x 60m, and 40m x 40m respectively. Tables I and II contain the system parameters of the C-130 microwave radiometer and scatterometer systems.

The WB-57 aircraft carries an X-band synthetic aperture radar (SAR) system. This system is a modified AN/APQ-102A military reconnaissance radar. Table III contains the performance parameters for this system.

The unique feature of this radar system is the ability to position the antenna to two different ranges of incidence angles. Figures 1 and 2 show these two modes of system operations.

## DATA ACQUISITION

To obtain the signature of oil-covered surface and non oil-covered surface without changing the radar viewing direction with respect to the wind direction the aircraft was flown orthogonal to the oil slick flow direction. Two passes across each of the two oil slicks (Burma-Agate on 11/15/79 and Ixtoc I on 1/29/80) were made to obtain a sufficient number of independent samples for statistical analyses. The aircraft flew at an altitude of 1500 feet over the Burma-Agate spill and 2000 feet over the Ixtoc I spill. Figure 3 is an aerial photograph obtained with a Zeiss nine-inch camera over the Burma-Agate. Figure 4 is an aerial photograph obtained over the Ixtoc I well site.

Of the microwave sensor data acquired, only the 13.3 GHz scatterometer systems and the C-band radiometer acquired data over both spills. Additional scatterometer data at 4.75, 1.6, and 0.4 GHz was obtained over the Burma-Agate spill and additional radiometer data at 18 GHz, 22 GHz, and 37 GHz was obtained over the Ixtoc I spill.

Although no ground truth was taken at either site, onboard observations indicated a calm sea with low surface-wind conditions. In addition, an estimate of the sea state was made using the non oil-covered surface 13.3 GHz scatterometer backscatter coefficient measurements and data presented by Jones.[16] This estimate indicated wind velocities of less than two meters per second for the Burma-Agate flights and between four meters per second and six meters per second for the Ixtoc I flights.

## SCATTEROMETER DATA ANALYSIS

By obtaining radar data across the oil slick, time histories of backscatter coefficient for each incidence angle of both oil-free and oil-covered surfaces provide measurements of the differences due to the presence of the oil. Figure 5 is a time history of 13.3 GHz 20-degree incidence angle backscatter coefficient for Run 2 of the Burma-Agate spill. The mean value of the non oil-covered surface is -8 dB while the mean value of the oil slick surface is -24 dB. Figure 6 is a time history of 13.3 GHz 20-degree incidence

angle backscatter coefficient for Run 3 of the Burma-Agate spill. The mean value of the non oil-covered surface is -9 dB while the mean value of the oil-slick surface is again -24 dB.

In both Figures 5 and 6, the radar return at 20-degrees incidence angle is decreased by about 16 dB due to the presence of the oil slick.

Figure 7 illustrates the angular and frequency dependence of this decrease in radar backscatter due to the presence of an oil slick on a smooth sea surface. The P-band (75cm) data is not included since the change in radar backscatter at the incidence angles being considered was negligible. The significant responses, greater than 6 dB due to the oil slick for 13.3 GHz and 4.75 GHz at 15- to 30-degrees incidence angles, are encouraging in that this range of angles has previously not been considered for oil slick detection.

Figure 8 is a time history of the 20-degrees incidence angle backscatter coefficient for the 13.3 GHz scatterometer and the microwave brightness temperature for the 18 GHz and 37 GHz radiometers for Run 2 of the Ixtoc I spill. Several significant features can be noted about the nature of this spill from Figure 8.

The higher value (-6 dB) of the backscatter coefficient at 20:55:20/27 is indicative of the return of non oil-covered surfaces with a surface wind speed estimated at six meters per second.[17] The decrease of the radar backscatter seen from 20:55:30 to 20:55:37 without a change in the radiometer brightness temperature is indicative of the smoothing action of an oil sheen (thickness of less than 0.1mm).[18]

The further decrease in the radar backscatter and the increase in brightness temperature seen from 20:55:40 through 20:55:45 is indicative of an oil slick (thickness approximately 1mm).[19,20]

Figure 9 is a comparison of 13.3 GHz radar backscatter coefficient versus incidence angle for various wind speeds over open ocean and oil spills. The decreases in backscatter for incidence angles less than 30 degrees is seen to be less for higher wind speeds. The 2m/sec data is from the Burma-Agate spill, the 6m/sec from the Ixtoc I spill and the 30m/sec data is from an earlier spill reported by Krishen.[15]

## RADIOMETER DATA DISCUSSION

Four radiometer data lines were selected because they highlight significant features of radio emission from an oil spill. Frequencies used in the data presented are C-, Ku-, and Ka-band (4.995 GHz, 18 GHz, and 37 GHz). Unfortunately, the 10.69 GHz scanner (Passive Microwave Imaging System) failed on the Ixtoc I mission and no data was obtained.

Figure 10 is a time history of C- and Ka-band brightness temperature from the Burma-Agate spill at incidence angles of 40 degrees. Both horizontal and vertical polarizations are shown. The Ka-band radiometer yielded the largest change in temperature. Review of the photographs from this flight line showed that the radiometers were turned on just as the aircraft started to pass over the oil slick. Immediately after the visible oil slick, there was an apparent clear area, then a small ship. The K-band radiometers, however, indicate that oil, though not visible to the camera was present, and clear water was not present until after the ship.

The next two Figures (11 and 12) are plots of data from the Ixtoc I spill with an incidence angle of 50 degrees. When looking at these figures, it should be noted that the C-band system looks ahead of the aircraft while the K-bands look behind the aircraft and thus a target appears in the K-bands approximately 20 seconds after it appears in the C-band. As in the Burma-Agate case, Figure 11 shows Ka-band data in which both the horizontal and vertical channels increase in brightness temperature. Ku- and K-band data (not shown) responded the same. Large quantities of oil were visible in a photograph of this area. Figure 12 shows the C-band results for the same area. At this incidence angle, the spill appears larger to the C-band radiometer's vertical channel. Part of this is possibly due to a larger antenna footprint for the C-band system.

However, the depression of the C-band horizontal channel is most interesting. It is believed that this is a function of wind velocity and the thickness of the oil on the surface.

Figure 13 is a plot of the data from three radiometers, C-, Ku-, and Ka-band made in the same area as the previous two figures, but at an incidence angle of zero degrees. Large quantities of oil were visible in a photograph of this area. Notice the lack of a significant return in the C-band data while Ka-band rises almost 20 degrees Kelvin.

Although no attempt has been made to determine the thickness of the oil from this data, thickness measurements have been made at other frequencies.[20] Perhaps this data will aid others in deciding the relative importance of radiometric data and what frequencies should be used.

## RADAR IMAGERY ANALYSIS

As stated previously, the radar imagery of the Ixtoc I spill was gathered as a part of the engineering evaluation of the system. Initial analysis of the data was more concerned with the ability of the radar systems to clutter-lock over water. The fact that the radar could image oil slicks was considered interesting, but radars had imaged oil slicks previously.

After analysis of the Burma-Agate and Ixtoc I scatterometer data produced the results shown in Figure 7, the radar imagery was again examined. This examination attempted to determine if the large decrease in backscatter at 20 degrees could be seen on the imagery.

Figure 14 is a radar image of the Ixtoc I slick taken in August 1979. This image was taken on a calm day. Winds in the area were five knots or less.

Plotted below the imagery are the quieting or decrease curves of Figure 7. Although the radar imagery was taken at X-band and the scatterometer data was taken at L-, C-, and Ku-band, it can reasonably be assumed that an X-band scatterometer would have produced a curve which would fall between the C-band and Ku-band curves.

Nadir is to the left of the image. The image spans a range of incidence angles from 14 degrees to 51 degrees. The brightness to the left of the image is typical of what happens to radar backscatter as you approach nadir. More and more energy is backscattered and less is forward scattered.

Note that the oil slicks still darken the image in this range, particularly around 20 degrees as predicted by the associated curves. The fact that the slicks are black indicates that the change is occurring over most of the grey scale of the film which is nominally 15 dB to 20 dB. This corresponds to the 10 dB to 15 dB quieting effect shown on the curve.

As noted previously, this imagery was taken on a relatively calm day. In discussing this imagery, NOAA representatives were quite surprised to see that the slicks could be seen on a calm sea. Their attempts to track the slicks with the U.S. Coast Guard AOSS system[6,7,13] had shown that at wind speeds less than five knots, slicks were not detectable.

This image and associated curves clearly show that the optimum range of incidence angles for oil-spill detection is in the 15 degrees to 25 degrees range. In this range, the larger surface return would place a less stringent power output requirement on the radar and the quieting effect of the oil is greatest for lower wind speeds.

## CONCLUSIONS

The data set used to prepare this paper was gathered under target of opportunity circumstances, thus all sensors were not available for all flights. However some general conclusions can be drawn. These are as follows:

(1) The presence of an oil spill on a water surface can be detected by a microwave radar system at incidence angles less than 45 degrees. Higher radar frequencies produce greater contrast between surfaces with and without oil on the surface. In the incidence angle range of 15 degrees to 25 degrees, there is greater surface return and maximum quieting due to the oil, thus reducing power output requirements on the radar.

(2) Windspeed over the surface affects the magnitude of the difference between oil-covered and non oil-covered surfaces. The use of low (<20°) incidence angles at low microwave frequencies (L-band) provides less detectibility than higher microwave frequencies (Ku-band).

(3) An X- or Ku-band synthetic aperture radar (SAR) operating at orbital altitudes and incidence angles similar to Seasat would provide an effective means for detecting, monitoring, and tracking large oil spills.

(4) More study must be given to the effects of sea state on the active microwave oil-spill signature at incidence angles less than 45 degrees.

(5) Radiometers, while not having the resolution capability that SAR systems have, do have potential for determining oil thickness on the surface.

## ACKNOWLEDGEMENTS

The authors would like to express their appreciation to Gordon C. Hrabal and James L. Lindemann of the NASA Lyndon B. Johnson Space Center Aircraft Operations Division for their assistance in gathering the basic data set for this paper; Jack M. Williams, Courtney E. Clements, and Joe R. Theriault of Lockheed Engineering and Management Services Company for C-130 Microwave Systems data reduction; and Joan P. Samonski of Lockheed Engineering and Management Services Company for the typing and editing of this paper.

## REFERENCES


1. Aukland, J. C., et al, 1971, Multi-sensor Oil Spill Detection: Proceedings Seventh International Symposium of Remote Sensing of Environment, pp 1045-1052.
2. Kennedy, J. M., Wermund, E. G., 1971, Oil Spills, Infrared and Microwave: Photogrammetric Engineering, pp 1235-1242.
3. Munday, J. C., MacIntyre, W. G., and Penney, M. E., 1971, Oil Slick Studies Using Photographic and Multispectral Scanner Data: Proceedings Seventh International Symposium of Remote Sensing of Environment, pp 1027-1043.
4. Aukland, J. C., Conway, W. H., and Sanders, N. K., 1969, Detection of Oil Slick Pollution on Water Surfaces with Microwave Radiometer Systems: Proceedings Sixth International Symposium of Remote Sensing of Environment, pp 789-796.
5. Thaman, R. R., Estes, J. E., Butler, R. W., and Ryerson, J. M., 1973, The Use of Airborne Imagery for the Estimation of Marine Oil Spills: An Operation Example: Proceedings Eighth International Symposium of Remote Sensing of Environment, pp 1093-1098.
6. Woolever, G. F., et al, 1975, Utilization of Remote Sensing Techniques for U.S. Coast Guard Missions: Proceedings Tenth International Symposium of Remote Sensing of Environment, pp 3-16.
7. Becker, R., 1972, Coast Guard Evaluates Oil Spill Detection Schemes, Microwave, May 1972, pp 12, 14.
8. Vizy, K. N., 1974, Detecting and Monitoring Oil Slicks with Aerial Photos: Photogrammetric Engineering, Vol. 40, pp 697-708.
9. Kotlarski, J. R., and Anderson, H. R., 1974, Oil Slick Detection by X-Band SAR: Proceedings Ninth International Symposium of Remote Sensing of Environment, pp 1775-1790.
10. Pilon, R. O., Purves, C. G., 1973, Radar Imagery of Oil Slicks: IEEE Transactions on Aerospace and Electronic Systems. Vol. AES-9, No. 5, September 1973, pp 630-636.
11. Kraus, S. P., et al, 1977, Radar Detection of Surface Oil Slicks: Photogrammetric Engineering and Remote Sensing, Vol. 43, No. 12, December 1977, pp 1523-1531.
12. Lund, T., 1978, Surveillance of Environmental Pollution and Resources by Electromagnetic Waves: D. Reidel Publishing Co., pp 309-318.
13. Maurer, A. T., Edgerton, A. T., and Meeks, D. C., 1977, U.S. Coast Guard Airborne Oil Surveillance System - Status Report: Proceedings Eleventh International Symposium of Remote Sensing of Environment, pp 1639-1640.
14. Guinard, N. W., 1971, The Remote Sensing of Oil Slicks: Proceedings Seventh International Symposium of Remote Sensing of Environment, pp 1005-1026.
15. Krishen, K., 1978, Detection of Oil Spills Using 13.3 GHz Scatterometer, Proceedings Eighth International Symposium of Remote Sensing of Environment, pp 1105-1119.
16. Jones, W. L., et al, 1977, Aircraft Measurements of the Microwave Scattering Signature of the Ocean: IEEE Transactions on Antennas and Propagation, January 1977, pp 52-61.

17. Moore, R. K., Fung, A. K., 1979, Radar Determination of Winds at Sea: Proceedings of IEEE, Vol. 67, No. 11, November 1979, pp 1504-1521.
18. Sabins, F. F., 1978, Remote Sensing, Freeman and Company, pp 334-342.
19. Smugge, T. J., 1979, The Use of Microwave Approaches in Hydrology: Proceedings of the American Society of Photogrammetry, pp 9-28.
20. Hollinger, J. P. and Mennella, R. A., 1973, Oil Spills - Measurements of Their Distributions and Volumes by Multifrequency Microwave Radiometery: Science Vol. 181, July 1973, pp 54-56.

TABLE I.- NASA/JSC C-13 AIRCRAFT MICROWAVE RADIOMETER SYSTEMS PARAMETERS

| Parameter | Bands | | | | | |
|---|---|---|---|---|---|---|
| | L | Ku | K | Ka | C | X(PMIS) |
| Frequency (GHz) | 1.4135 | 18 | 22.05 | 37 | 4.995 | 10.69 |
| Bandwidth (MHz) | 27 | 200 | 200 | 500 | 50 | 150 |
| Sensitivity (degrees) | 1 | 1 | 1 | 1 | 1 | 1 |
| Integration Time (seconds) | 0.1 | 0.1 | 0.1 | 0.1 | 0.1 | Variable |
| Antenna Type | Phased Array | Horn | Horn | Horn | 3-foot Dish | Phased Array (a) |
| Beam Width (3 dB) | 16° | 4° | 4.5° | 4° | 5° | 1.6° x 2.6° |
| Polarity | Either H or V | Sim. H & V | Sim. H & V | Sim. H & V | Sim. H & V | Sim. H & V |
| Incidence Angle (degrees) | 0 - 50 | 0 - 50 | 0 - 50 | 0 - 50 | 0 - 50 | 49.5 (a) |

(a) Scans constant incidence angle.

TABLE II.- NASA/JSC C-130 SCATTEROMETER SYSTEMS PARAMETERS

| Parameter | Bands | | | |
|---|---|---|---|---|
| | Ku | C | L | P |
| Frequency (GHz) | 13.3 | 4.75 | 1.6 | 0.4 |
| Polarization | VV | VV or HH and CROSS | VV or HH and CROSS | VV or HH and CROSS |
| Along-track Resolution (feet) | 120 | 120 | 120 | 240 |
| Cross-track Beamwidth (degrees) | 2.5 | 4 | 8 | 16 |
| Incidence Angles (degrees) | 5-50 | 5-50 | 5-50 | 5-50 |
| Nominal Bandwidth (Hz) ($\theta$ = 30° Vel = 150 kts) | 400 | 150 | 50 | 12 |
| Nominal Integration Time per Measurement (seconds) | 0.16 | 0.32 | 0.64 | 1.0 |
| Number of Measurements Averaged per Second | 6 | 3 | 1.5 | 1.0 |
| Precision of Measurement per Second of Spatial Data (dB) ($\theta$ = 30°) | +0.36<br>-0.38 | +0.57<br>-0.62 | +1.0<br>-1.1 | +2.0<br>-2.6 |



C-3

TABLE III.- X-BAND SIDE-LOOKING RADAR SYSTEM PARAMETERS

| | |
|---|---|
| Transmit Frequency | 9600 MHz |
| Transmit Output Power | 50 KW |
| Transmit Polarization | Selectable Horizontal or Vertical |
| Pulse Width (half power) | 0.90 Micro-second |
| Pulse Repetition Frequency (PRF) | Variable with Ground Speed (at 400 knots, PRF is 1352 PPS) |
| Pulse Spectrum Bandwidth | 15 MHz |
| Antenna Stabilization Limits | Up 4.5°, Down 2.5°<br>Azimuth ±6.75°<br>Roll ±3° |
| Swath Coverage at 60,000 Feet | Mode I - 2.5 to 12.5 Miles<br>Mode II - 10 to 20 Miles |
| Range Resolution | <50 Feet |
| Azimuth Resolution | <50 Feet |
| Azimuth Beamwidth | 1.45° one way - half power |
| Receivers | One Vertical, One Horizontal (Hardwired to Recorder) |
| Recording Mode | Optical and Selected Digital |

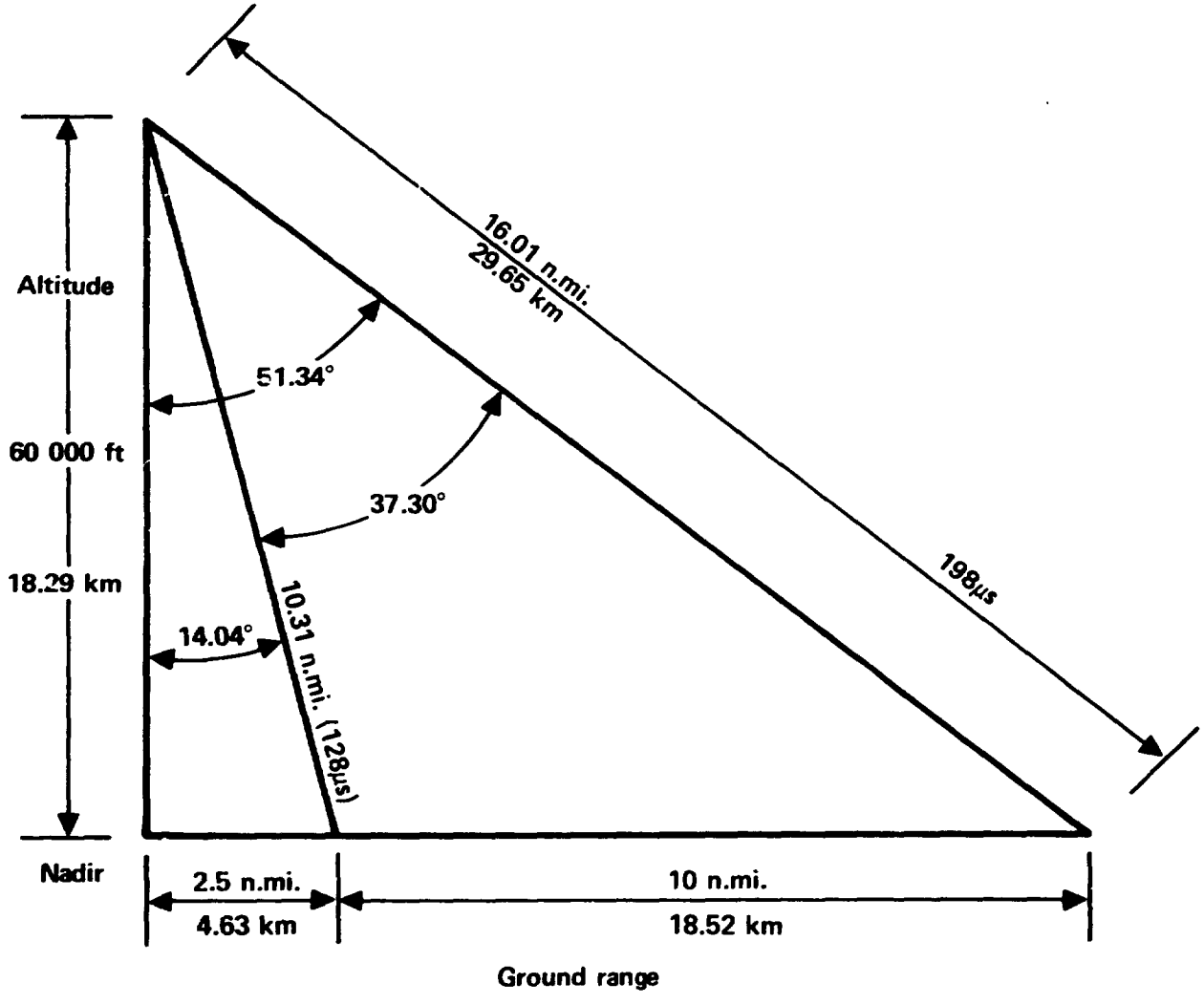


Figure 1.— Mode I, dual polarized X-SAR.

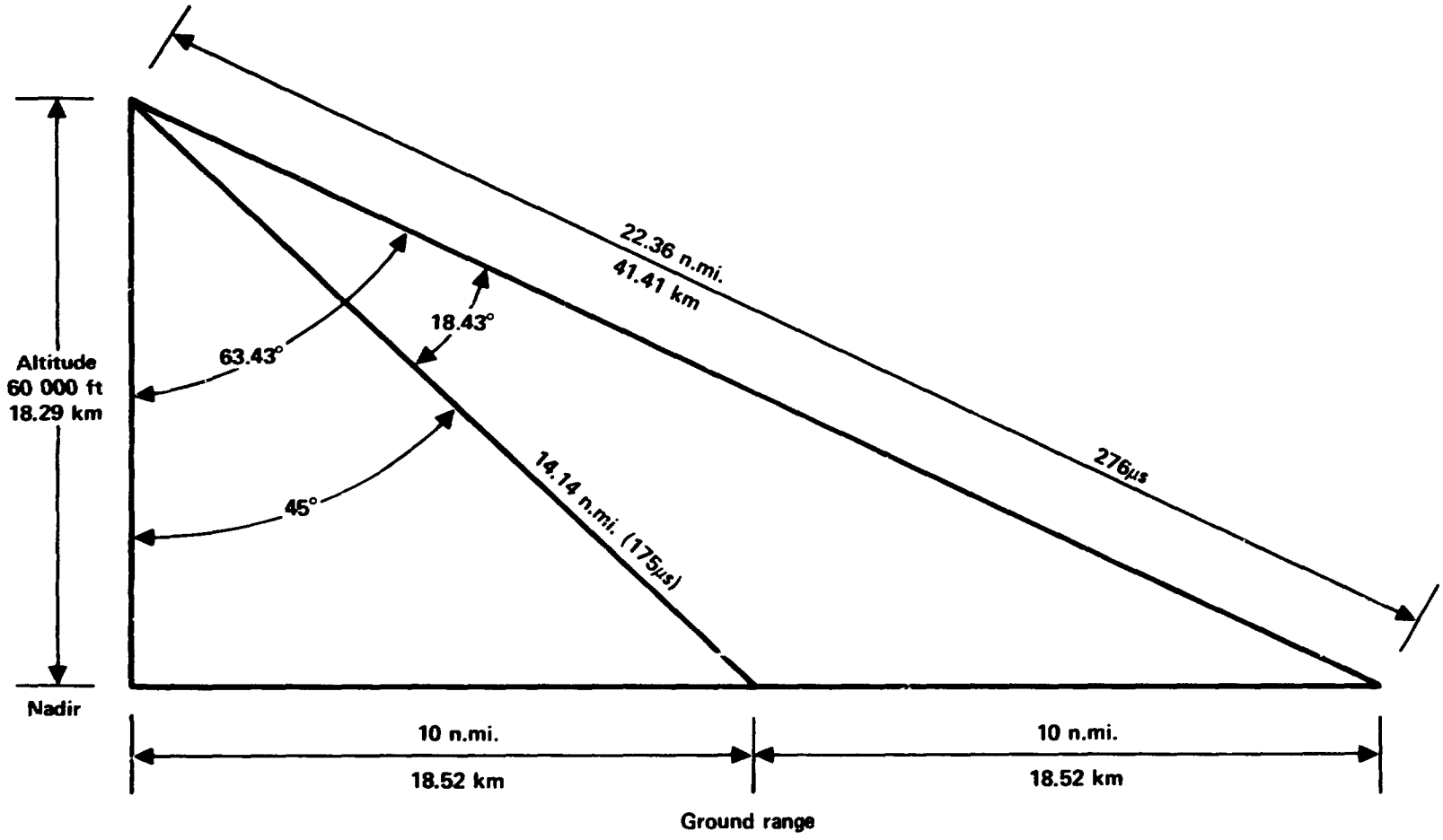


Figure 2.— Mode II dual polarized X-SAR.

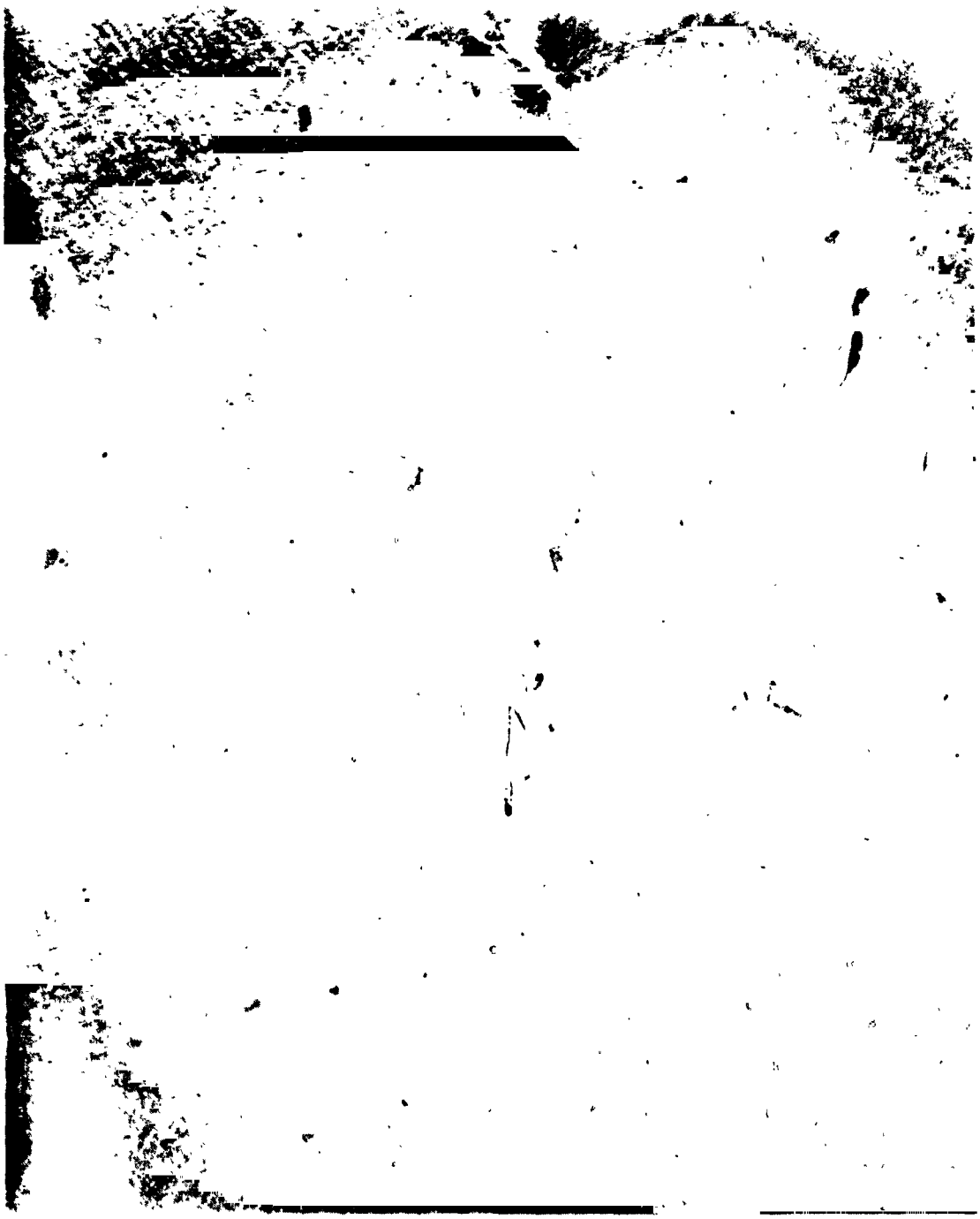

Figure 3.- Aerial photograph of the Burma-Agate.

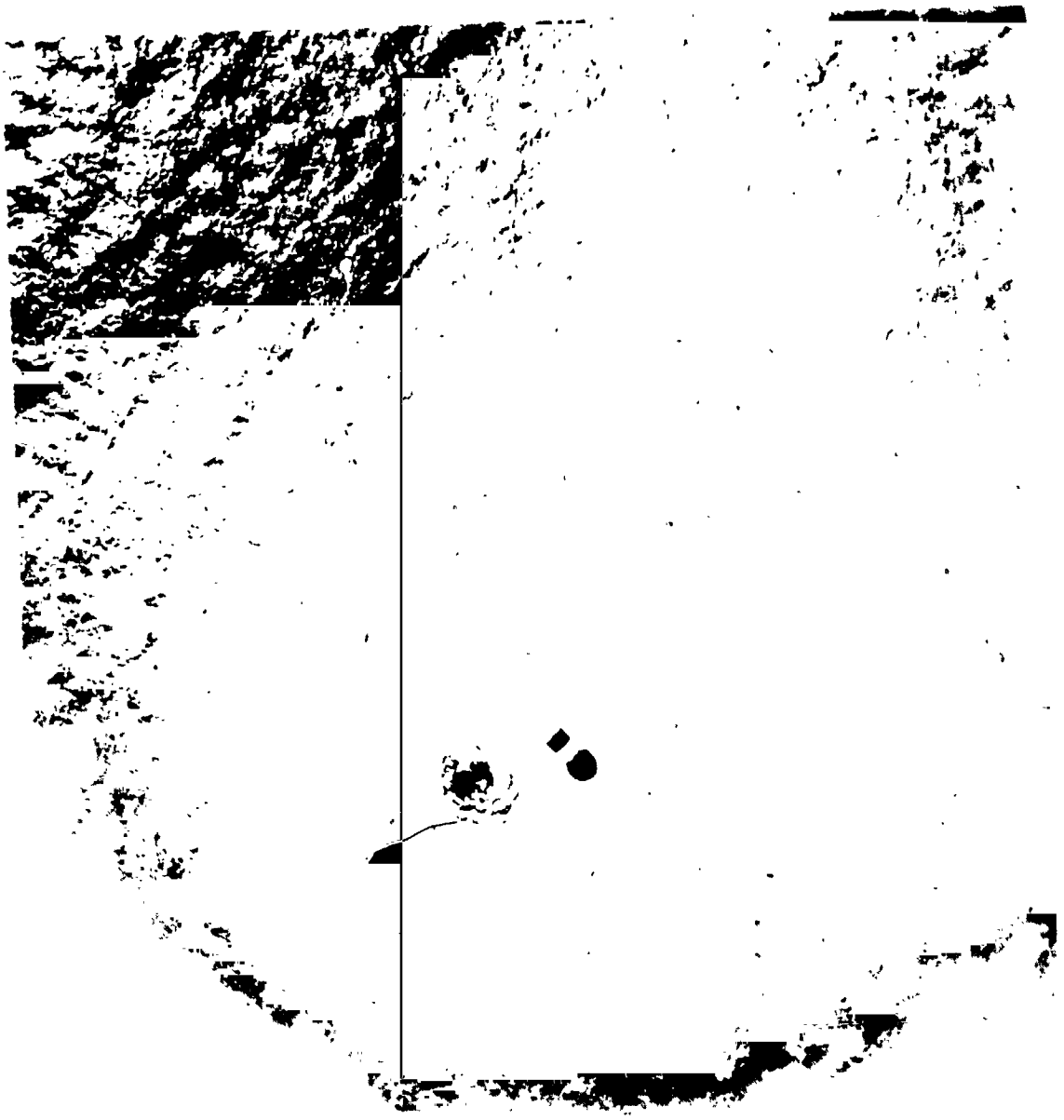

Figure 4.- Aerial photograph of the Ixtoc I well.

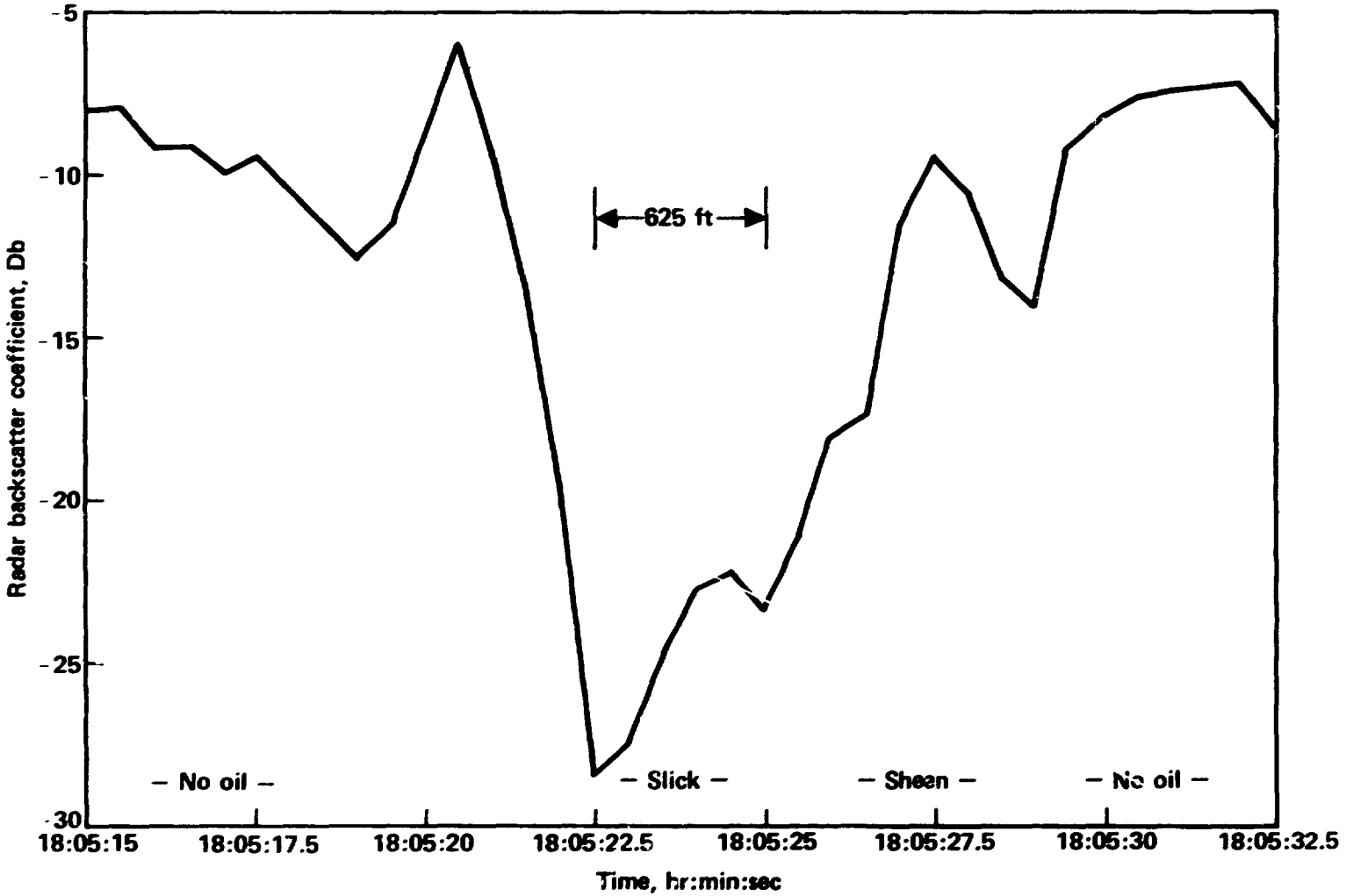


Figure 5.— Time history - 13.3-GHz scatterometer, 20° incidence angle backscatter coefficient for run 2, Burma-Agate oil spill.

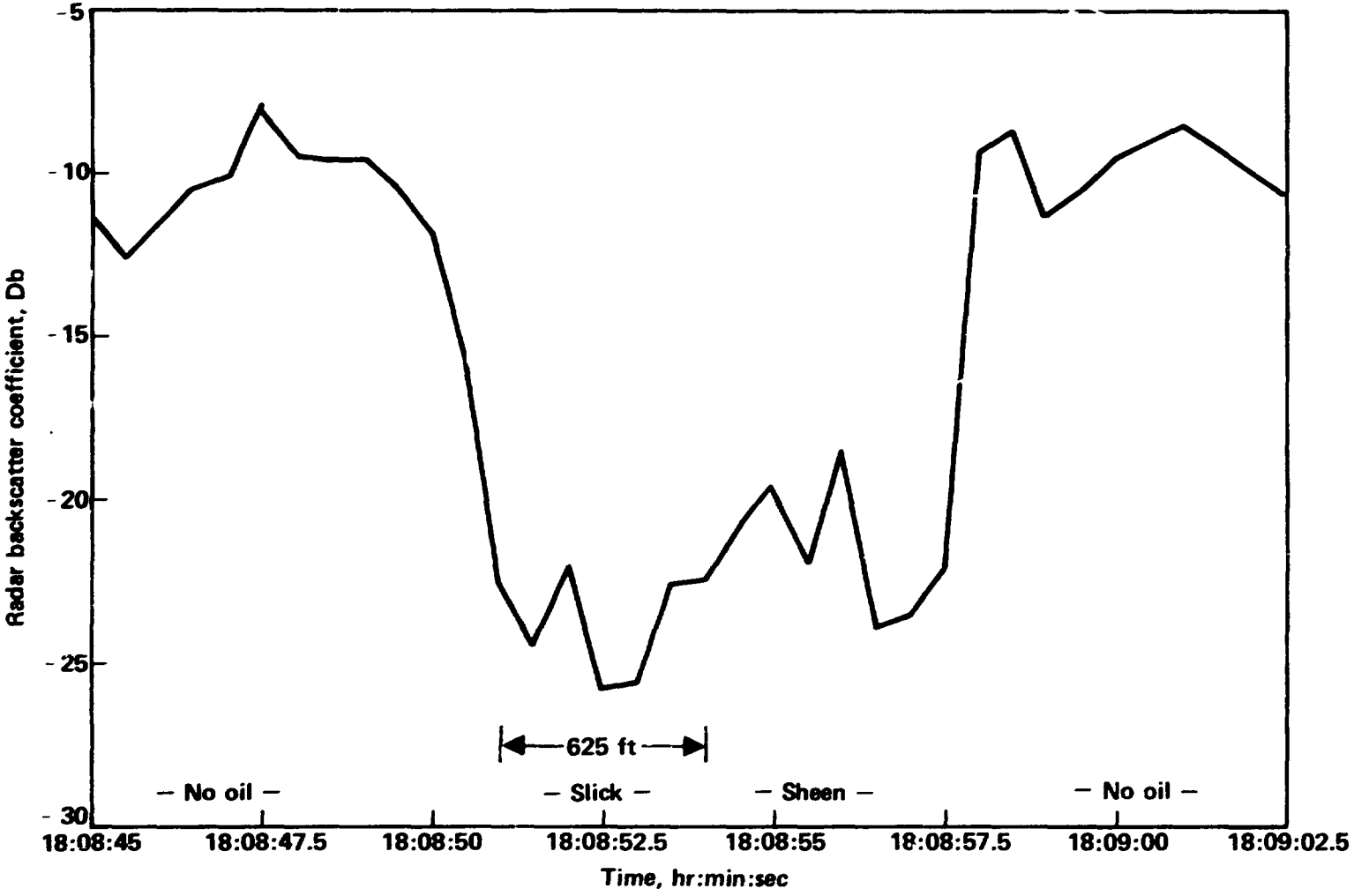


Figure 6.— Time history - 13.3-GHz scatterometer, 20° incidence angle backscatter coefficient for run 3, Burma-Agate oil spill.

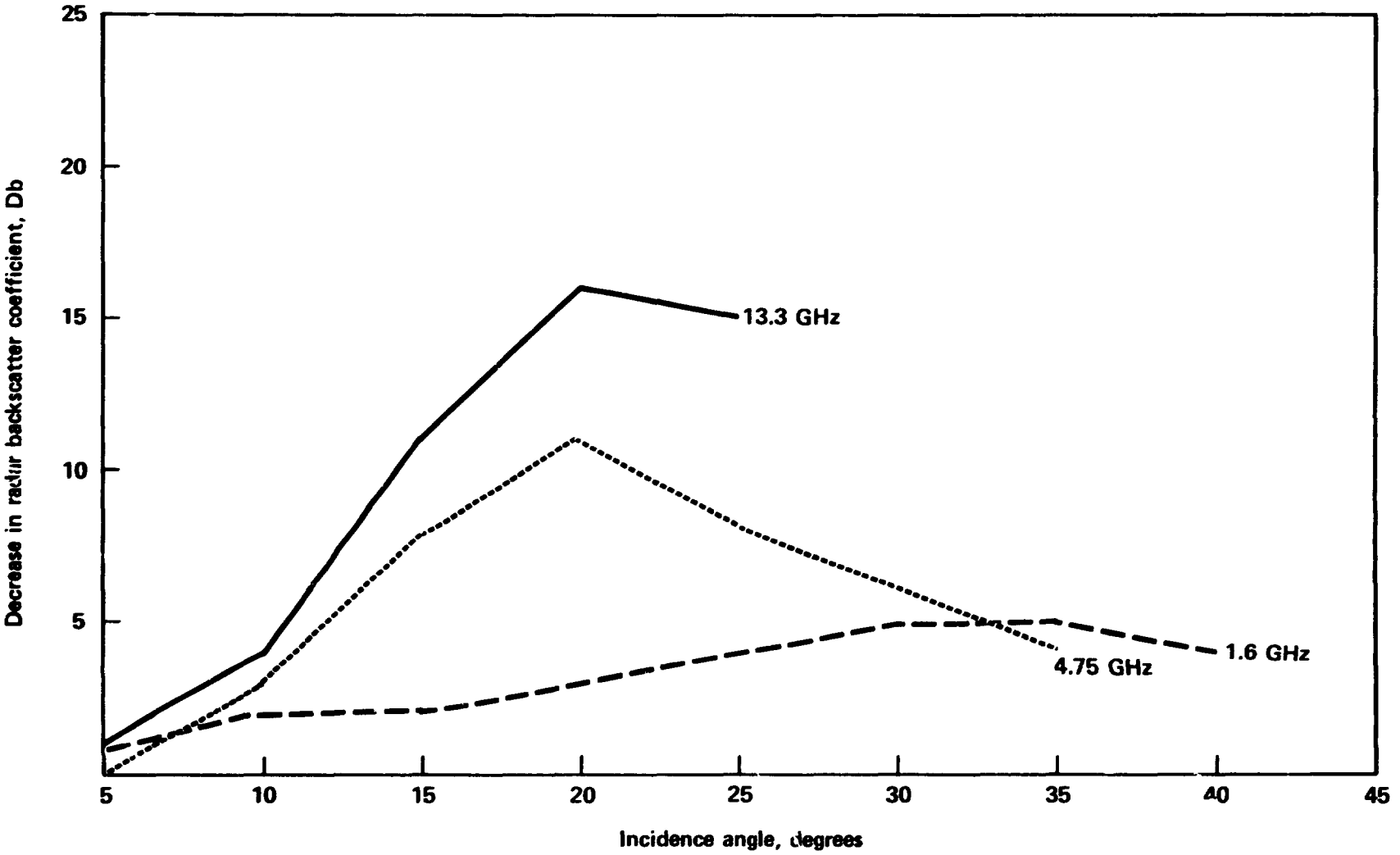


Figure 7.— Decrease in backscatter coefficient for 13.3-GHz, 4.75-GHz, 1.6-GHz scatterometer data versus incidence angle due to presence of oil slick on smooth sea surface, Burma-Agate oil spill, Runs 2 and 3.

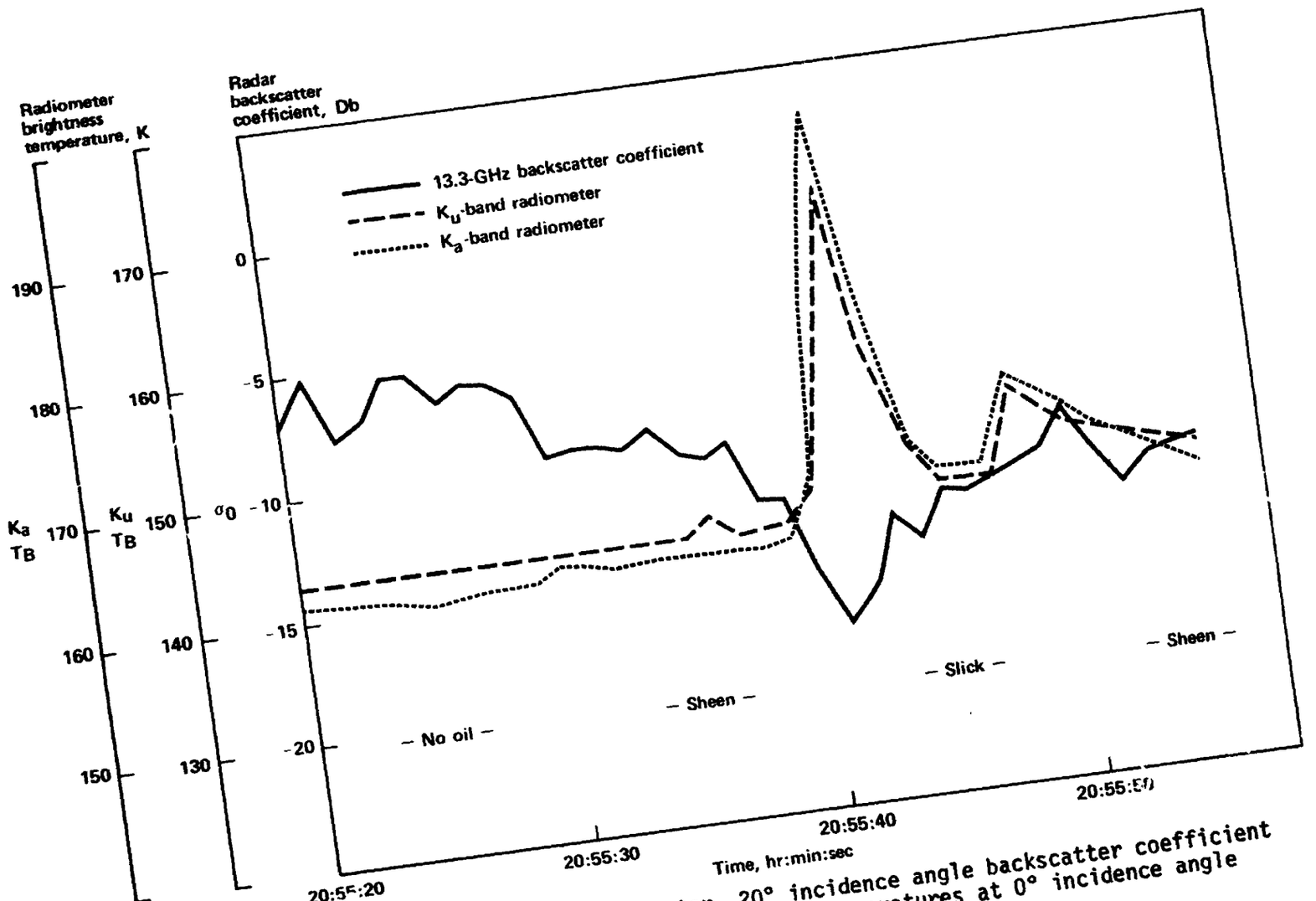


Figure 8.— Time history - 13.3-GHz scatterometer, 20° incidence angle backscatter coefficient and 18-GHz ($K_u$) and 37-GHz ($K_a$) radiometer brightness temperatures at 0° incidence angle for run 2, IXTOC I oil spill.

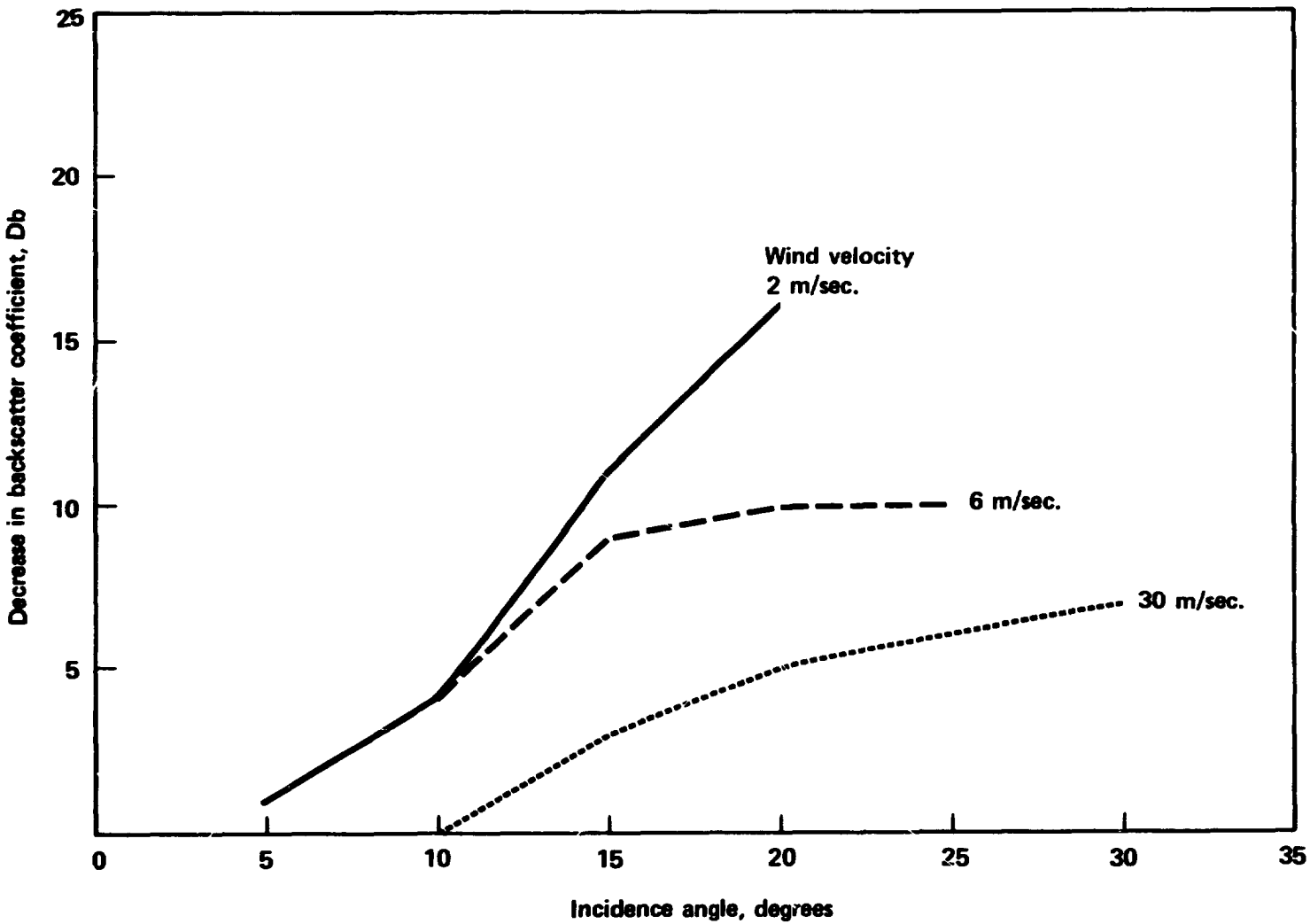


Figure 9.— Decrease in backscatter coefficient for 13.3-GHz scatterometer versus incidence angle due to presence of oil slick for various windspeed conditions.

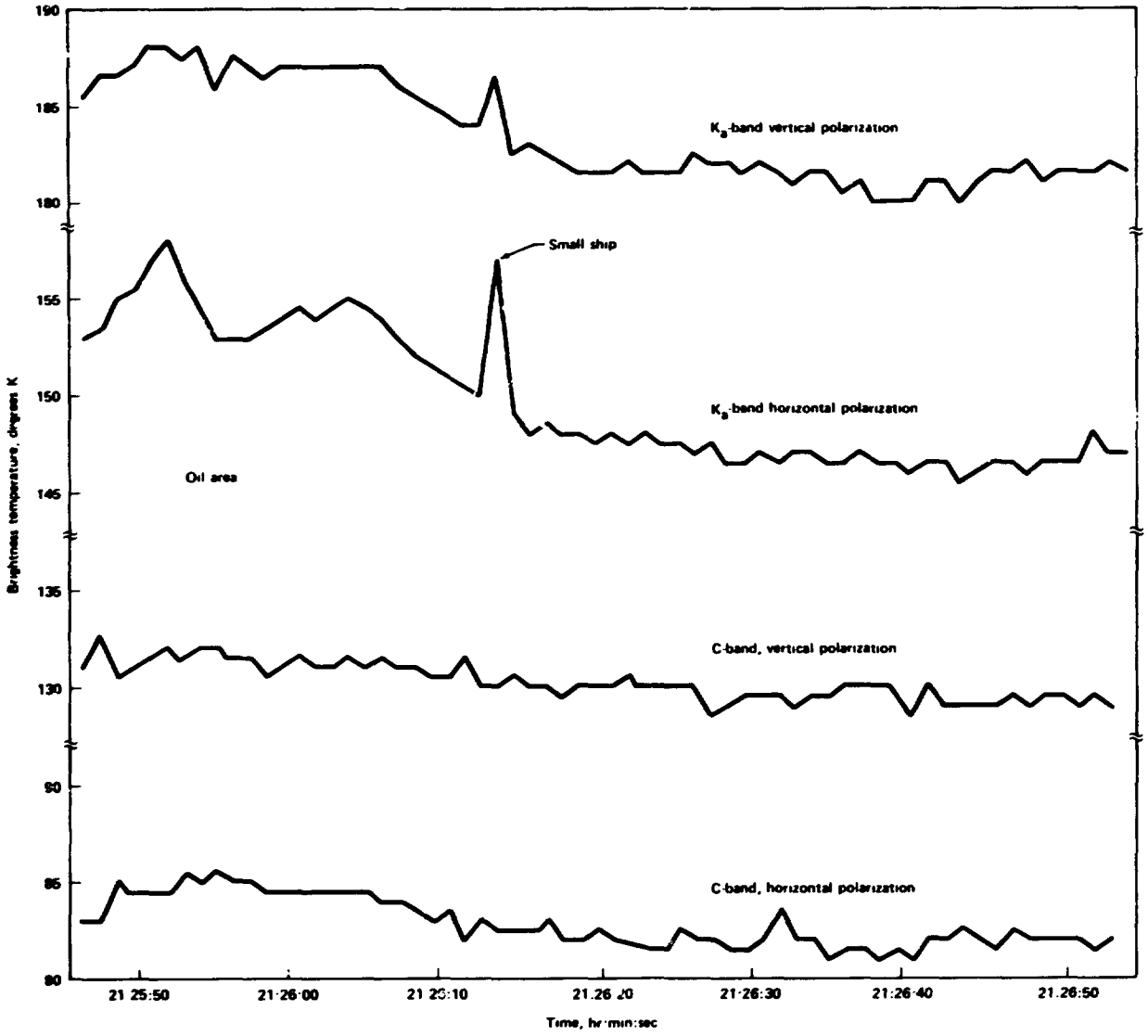


Figure 10.— Time history of C-band and $K_a$-band radiometer brightness temperature, 40° incidence angle, Burma Agate oil spill.

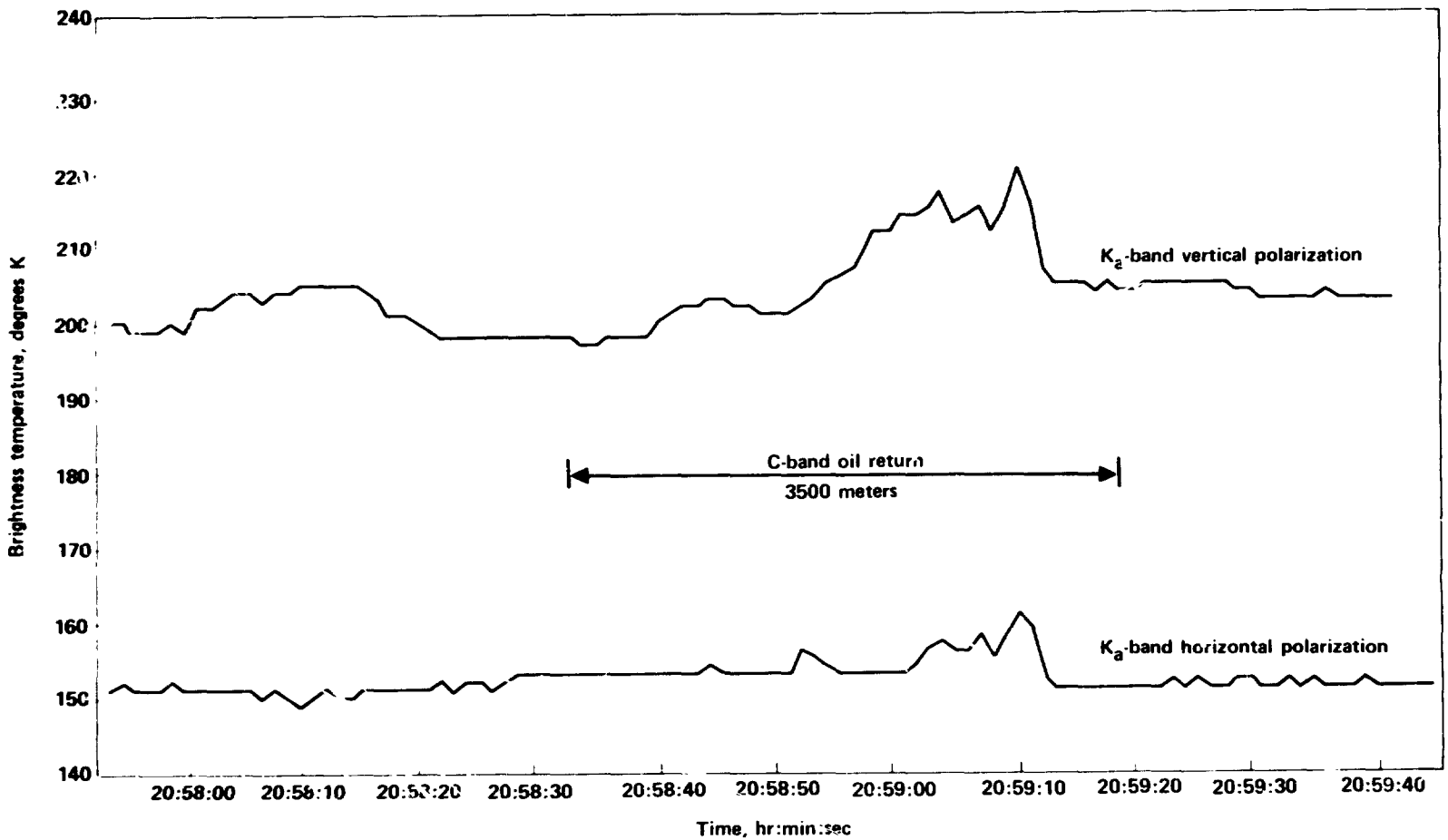


Figure 11.— Time history of $K_a$-band radiometer brightness temperature, $50^{\circ}$ incidence angle, IXTOC I oil spill.

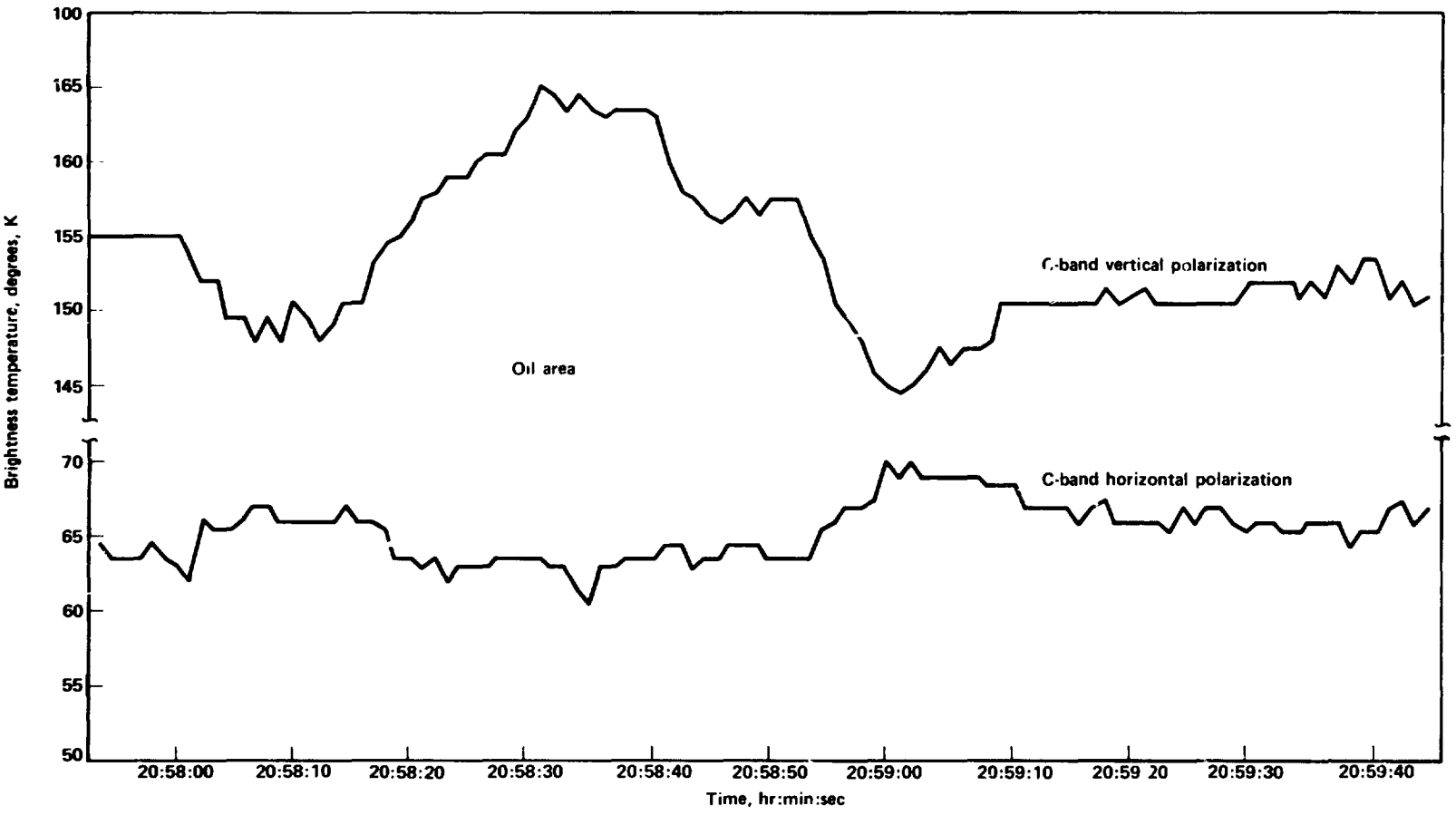


Figure 12.— Time history of C-band radiometer brightness temperature, 50° incidence angle, IXTOC I oil spill.

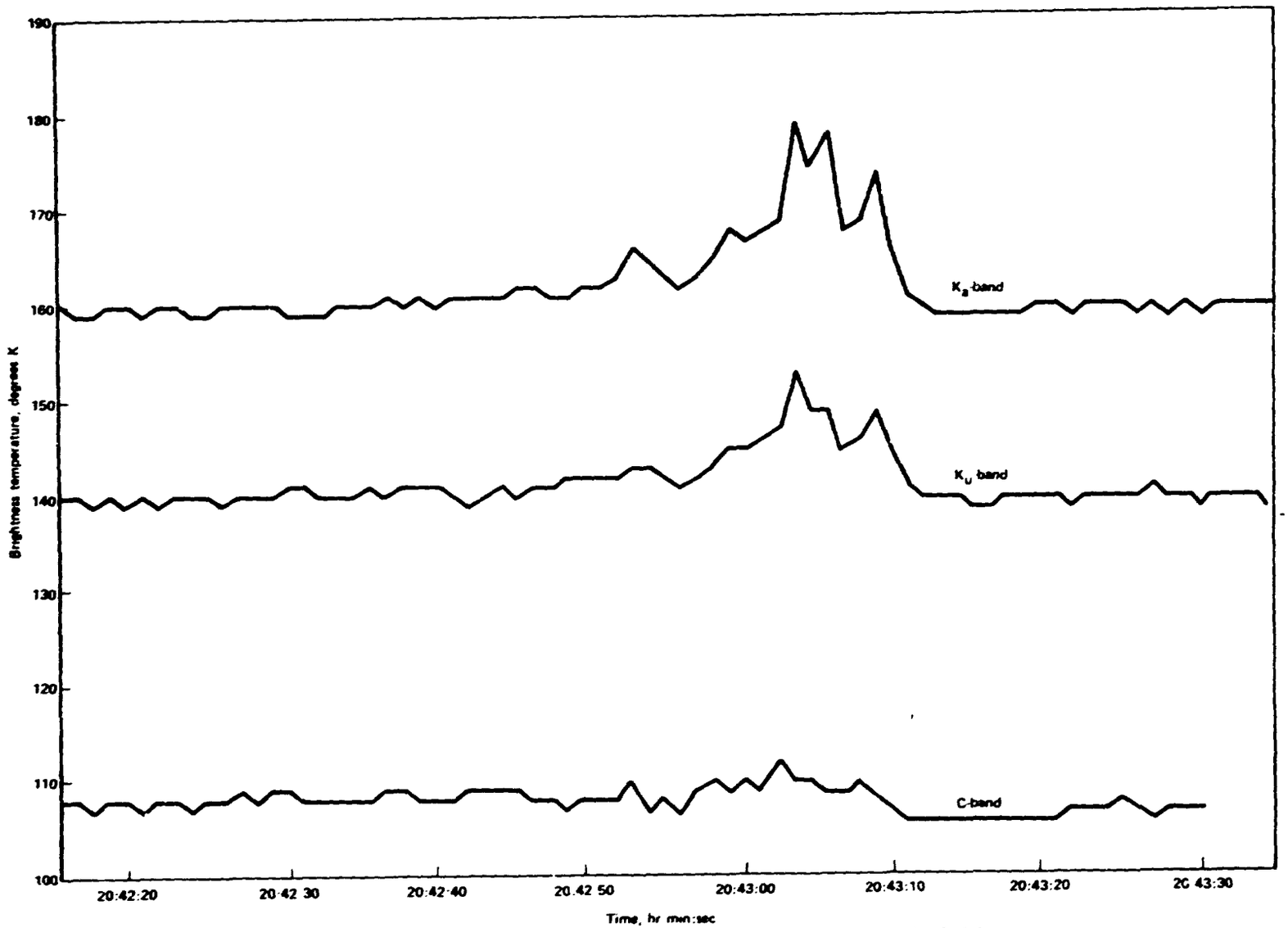


Figure 13.— Time history of C, $K_a$ and $K_u$ band radiometer brightness temperature, $0^o$ incidence angle, IXTOC I oil spill.

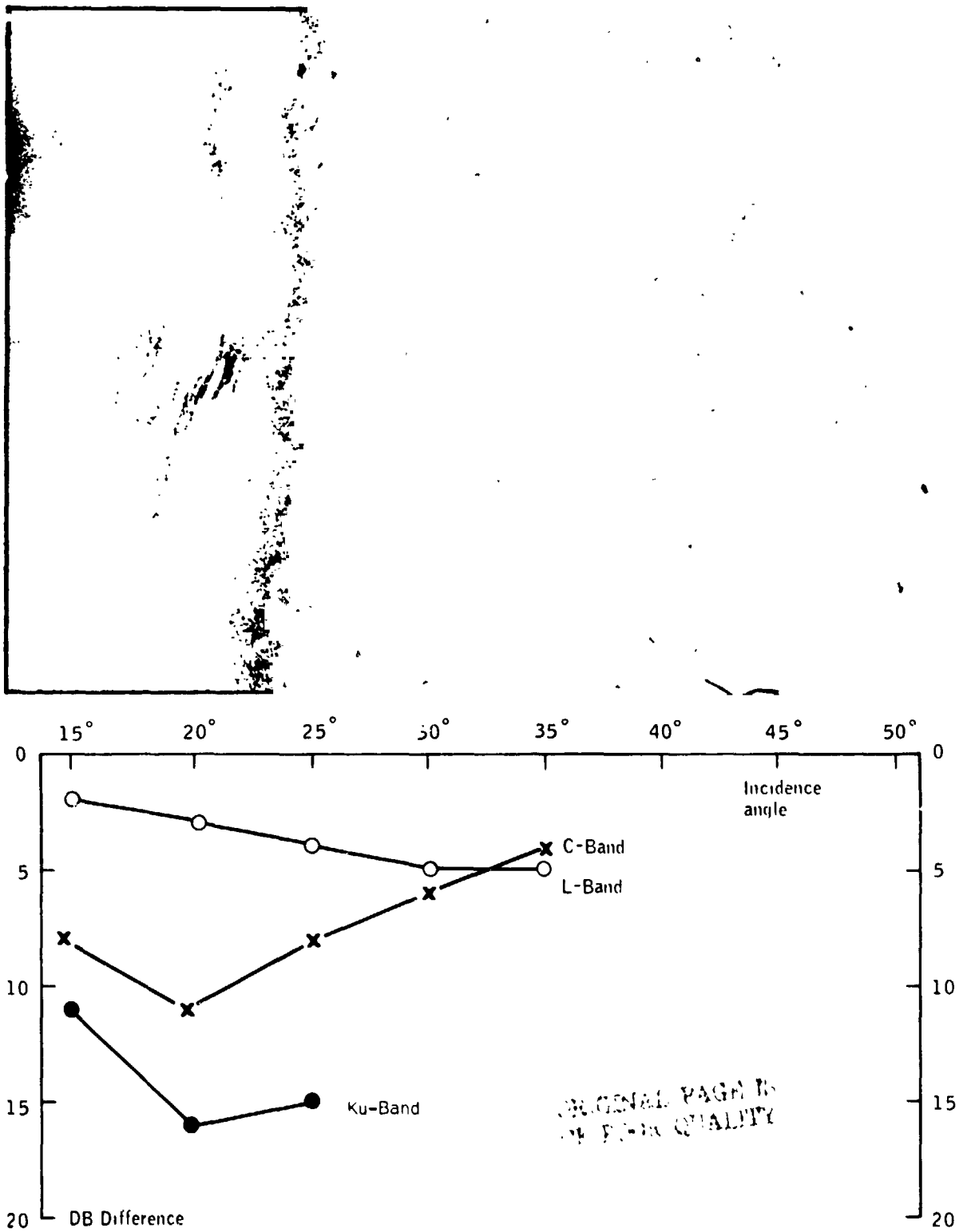


Figure 14.- Comparison of Radar Imagery and Decrease in Scattering Coefficient Curves.